Physics Letters A 376 (2012) 753–757

Contents lists available at SciVerse ScienceDirect

Physics Letters A

www.elsevier.com/locate/pla

Self-organized criticality in MHD driven plasma edge turbulence

G.Z. dos Santos Lima [a,*], K.C. Iarosz [b], A.M. Batista [b], I.L. Caldas [c], Z.O. Guimarães-Filho [d], R.L. Viana [e], S.R. Lopes [e], I.C. Nascimento [c], Yu.K. Kuznetsov [c]

[a] Escola de Ciências e Tecnologia, Universidade Federal do Rio Grande do Norte, 59014-615, Natal, RN, Brazil
[b] Programa de Pós-Graduação em Física, Universidade Estadual de Ponta Grossa, 84030-900, Ponta Grossa, PR, Brazil
[c] Instituto de Física, Universidade de São Paulo, 05508-090, SP, Brazil
[d] IIFS/PIIM, Université de Provence, France
[e] Departamento de Física, Universidade Federal do Paraná, 81531-990, Curitiba, PR, Brazil

ARTICLE INFO

Article history:
Received 9 September 2011
Received in revised form 15 November 2011
Accepted 15 December 2011
Available online 17 December 2011
Communicated by F. Porcelli

Keywords:
Plasma
Turbulence
Self-organized criticality
MHD activity

ABSTRACT

We analyze long-range time correlations and self-similar characteristics of the electrostatic turbulence at the plasma edge and scrape-off layer in the Tokamak Chauffage Alfvén Brésillien (TCABR), with low and high Magnetohydrodynamics (MHD) activity. We find evidence of self-organized criticality (SOC), mainly in the region near the tokamak limiter. Comparative analyses of data before and during the MHD activity reveals that during the high MHD activity the Hurst parameter decreases. Finally, we present a cellular automaton whose parameters are adjusted to simulate the analyzed turbulence SOC change with the MHD activity variation.

1. Introduction

In tokamaks and stellarators [1], the plasma edge electrostatic turbulence is the main cause of the anomalous particle and energy transport that limits the magnetic confinement performance [2,3]. Despite the expressive progress that has been achieved in the last decades, much investigation is still necessary to better understand and to control the electrostatic turbulence in tokamaks.

Fluctuation spectrum [4], recurrence [5–7], and self-organized criticality (SOC) [8,9] are among subjects recently investigated to determine basic statistical properties of the electrostatic plasma turbulence and transport [10]. In particular, evidences of SOC, that bring together the ideas of self-organization of nonlinear dynamics systems with the often observed near-critical behavior [11,12], have been found in the tokamak plasma turbulence experimentally [8] and in numerical simulations [10].

Some features of turbulence observed in all tokamak discharges can be computationally investigated, independent of any physical model to interpret the turbulent fluctuations, by the SOC dynamics of cellular automata models of running sandpile dynamics [13]. Similar models have been applied to study self-organization in other dynamical systems, as cancerous cells proliferation [14], traffic flow [15], neural network [16], ecosystems [17], and spatial pattern formation [18]. In these models avalanche events appear naturally and can account for some specific SOC features [19].

In the tokamak TCABR, when the MHD activity increases it synchronizes with the electrostatic fluctuations and their frequency spectra have the same peaks [20,21]. The high MHD activity modifies the plasma turbulence leading to a new dynamic scenario in the plasma edge. The main differences in the turbulence with low and high MHD activities have been recently analyzed [8,19,22]. In this Letter we report alterations on the turbulence SOC behavior whenever the MHD activity increases in TCABR.

In our analyzes of the plasma edge turbulence in TCABR tokamak, with low and high MHD activity, we find that the obtained power spectra, autocorrelation, and Hurst parameter radial profiles are compatible with those expected for turbulent fluctuations with SOC dynamics. Besides that, we find that during the turbulence driven high MHD activity the Hurst parameter, a relevant SOC indicator, decreases in all frequency range. Moreover, we simulate all the described characteristics and changes obtained in the analyzed data with a modified cellular automaton which is a sandpile model with an external perturbation. We also find that during the high MHD activity the Hurst parameter of the electrostatic turbulence decreases.

This Letter is organized as follows: in Section 2 we present the experimental setup. Section 3 shows the radial dependence of SOC in the experimental results. Section 4 treats the self-organized criticality during MHD driven turbulence. Section 5

* Corresponding author.
E-mail address: gzampier@ect.ufrn.br (G.Z. dos Santos Lima).

0375-9601/$ – see front matter
doi:10.1016/j.physleta.2011.12.026

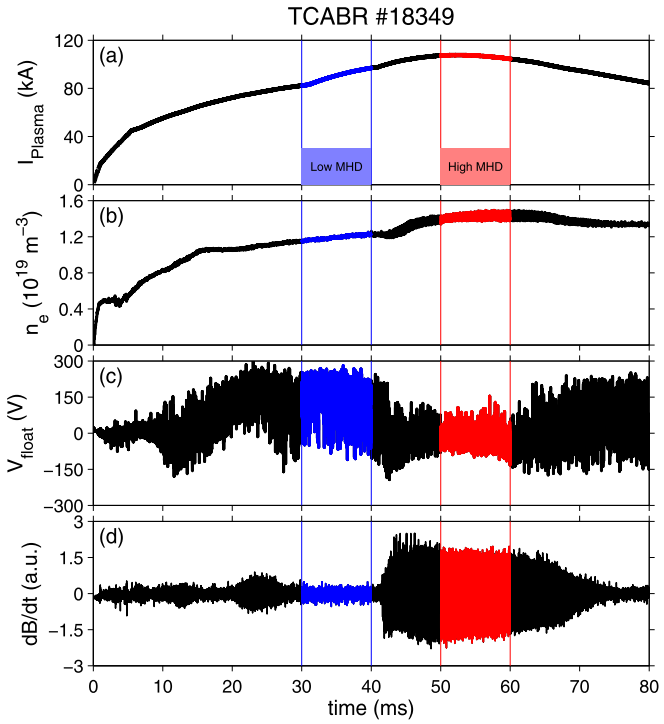

Fig. 1. Time evolution of plasma discharge in TCABR tokamak. (a) Plasma current, (b) central chord plasma mean density, (c) floating electrostatic potential for a typical discharge inside the limiter ($r = 17$ cm), (d) ion saturated current from the vertical lines indicate the analyzed time interval.

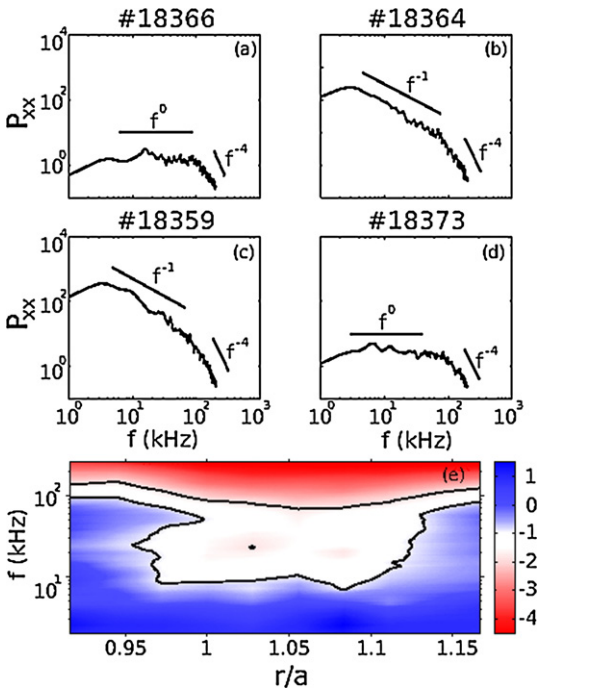

Fig. 2. Power spectrum P_{xx} of the floating potential fluctuation at four different radial positions: (a) $r/a = 0.91$ (inside the plasma column); (b) $r/a = 1.00$ (limiter); (c) $r/a = 1.05$ and (d) $r/a = 1.16$ (outside the plasma column), respectively. (e) Local decay exponent in function of the frequency and the radial position obtained from 28 shots. (For interpretation of the references to color in this figure, the reader is referred to the web version of this Letter.)

shows a theoretical model that we use to simulate the behavior observed in experiments. The last section presents the conclusions.

2. Experimental setup

The experiments are done in TCABR [23], a small size tokamak (major radius $R = 0.6$ m, minor radius $a = 0.18$ m, central toroidal magnetic field $B_0 = 1$ T) in which the MHD activity can increase and saturates without disruptions by an appropriated selection of the plasma current evolution [20,22] or by biasing an electrode inserted at the plasma edge [24].

The turbulence is measured at the edge and the scrape off layer (SOL) regions by Langmuir probes. The floating potential configuration is recorded with an acquisition rate of 1 MHz. The probes can be moved between successive shots in the radial position ranging from $r = 16.5$ to 21 cm (corresponding to r/a between 0.92 to 1.17). Fig. 1 shows the typical evolution of the plasma during the discharges considered in this work. As it can be seen in Fig. 1, in the interval from 30 to 40 ms, the plasma current increases, while the MHD activity is low and the fluctuating potential and density are almost stationary. But, after the time 40 ms, the MHD activity amplitude starts increasing and saturates by the time 50 ms. In the interval from 50 to 60 ms, during the MHD activity enhancement, the plasma density reaches a second plateau. For all the analyzed discharges, we selected two time intervals corresponding to the low and high MHD activity conditions [25]. We choose the first time windows in the almost stationary stage just before the growth of the MHD activity (50 ms–60 ms for the shot in Fig. 1). Complementary, we select a second time window during the interval with saturated high MHD activity.

3. Self-organized criticality radial dependence

The first objective of this study is to verify the existence of SOC dynamics in the plasma edge region of TCABR during the usual low MHD activity [26–28] (as commonly observed in other tokamaks), and to evaluate how this dynamic is dependent of the radius [29]. In order to perform it, we analyze some typical features associated with SOC dynamics in the floating electrostatic potential, such as: power spectrum (Fig. 2), autocorrelation function (ACF) (Fig. 3) and the Hurst parameter of the fluctuations (Fig. 4).

In SOC systems, the power spectra are expected to be nearly $1/f$ noise for a given range of frequencies [11], separated by two frequency intervals quite different, at least in our case [29]. For the TCABR tokamak data from the inside plasma column at $r/a = 0.91$ [Fig. 2(a)] and far outside for $r/a = 1.16$ [Fig. 2(d)], the frequency spectra show two distinct frequency intervals range with approximate decay slope of 0 and -4. The spectral decay with the $1/f^4$ dependence occurs for high frequencies ($\geqslant 200$ kHz) while the $1/f^0$ spectral dependence occurs for low frequencies ($\leqslant 100$ kHz). The turbulence in these positions does not show evidences of SOC dynamics. However, in Fig. 2(b) for $r/a = 1.00$ and (c) for $r/a = 1.05$ we can observe the $1/f$ spectral dependence ($3\text{ kHz} \leqslant f \leqslant 100$ kHz). In order to evaluate the spectral range in which the decay slope is close to -1, we fit the slope of the power spectra considering only a small range of the frequency spectra.

By doing it, we determine the local slope in function of the radial position and mean frequency of each frequency range used to determine the local slope. The radial dependence of the decay slope obtained from the fit of 28 shots is summarized in Fig. 2(e). The black contour lines in Fig. 2(e) limit the region in which the local slope is close to -1: the regions with local slopes close to -1 are marked in white, while slopes below -1 are indicated in red and the blue is used to mark the regions with slopes above -1. As it can be seen in Fig. 2(e), a broad frequency range in which the slope is close to -1 is observed for the radial positions close to the plasma edge ($0.97 < r/a < 1.13$), while only a narrow frequency range with slope close to -1 is observed in the most internal ($r/a \sim 0.93$) and external ($r/a \sim 1.16$) positions

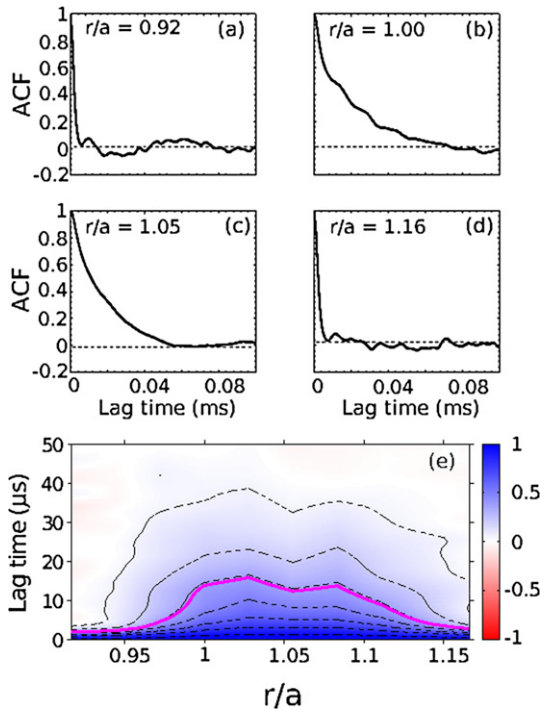

Fig. 3. Autocorrelation function (ACF) of the floating potential fluctuations measured at four different radial positions: (a) $r/a = 0.91$ (inside the plasma column); (b) $r/a = 1$ (limiter); (c) $r/a = 1.05$ and (d) $r/a = 1.16$ (outside the plasma column), respectively. (e) Average ACF obtained from 28 shots. The thick magenta contour line indicates the $\exp(-1)$ level and the dashed black contour lines the levels of $0.05, 0.20, 0.35, \ldots, 0.95$. (For interpretation of the references to color in this figure, the reader is referred to the web version of this Letter.)

measured by the probes. These figures suggest that the SOC is radial dependent. Similar frequency dependency was also observed in other experimental observations in which the ion saturation current was measured at the radial position where the flow was zero [13].

The autocorrelation functions (ACF) of the floating potential fluctuations measured at the same four radial positions: (a) $r/a = 0.91$ (inside the plasma column); (b) $r/a = 1.00$ (limiter); (c) $r/a = 1.05$ and (d) $r/a = 1.16$ (outside the plasma column), respectively, are displayed in Fig. 3. In Fig. 3(a) and Fig. 3(d), it can be seen that the value of ACF decays very rapidly with time, showing the short decorrelation time of the local turbulence in the two considered radial positions. However, in Figs. 3(b) and 3(c) we observe the existence of long time correlations with evidence of a tail in the ACF near the limiter ($r/a = 1.00$). In fact, these results show the radial dependence of the e-folding time as reported in [8].

A better characterization of the radial dependence of the ACF is presented in Fig. 3(e), which shows the average ACF in each radial position taken from the same 28 shots used to produce Fig. 2(e). Dashed black contour lines indicates the correlation levels of $0.05, 0.20, 0.35, \ldots, 0.95$ while the magenta thick contour line indicates the $\exp(-1) \sim 0.37$ level. The autocorrelation function displays an extended tail at large delay time near to the limiter, enforcing the evidence that this is a region with high SOC behavior.

Other evidence of self-organized criticality on TCABR fluctuations is obtained through the Hurst parameter (with R/S method) [30]. The Hurst parameter is defined as $E[R(n)/S(n)] = \lambda n^H$ ($n \to \infty$), where E is the expected value, $[R/S]$ is the rescaled range, n is the number of data points and λ is a constant. The Hurst parameter of the time series gives us the degree of the regularity or randomness and long-time effect of the process, contributing to the knowledge of the future behavior of the system

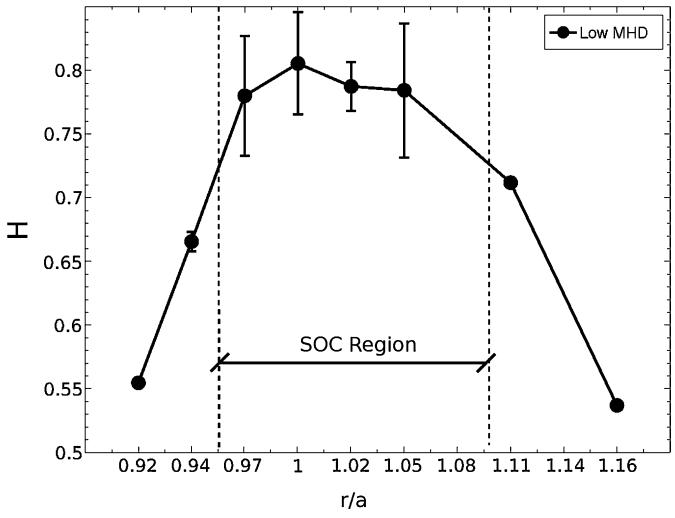

Fig. 4. Radial dependence of the Hurst parameter (circles). The vertical black dashed lines mark the position of the existence of SOC behavior.

and characterizing how the process is self-organized criticality [31,32]. The value of the Hurst parameter varies between 0 and 1. For $H = 0.5$, the process is random. Moreover, for $0 \leqslant H \leqslant 0.5$ the time series is characterized like anti-persistent or anti-correlated, and for $0.5 < H \leqslant 1$ the signal are persistent or auto-correlated. Fig. 4 shows the radial dependence of the Hurst parameter for the time interval with low MHD activity. Consistently Figs. 2, 3 and 4 point out that the region near to the plasma limiter shows strong evidences of the SOC behavior. So, in the following analysis the region with r/a between 0.95 and 1.1 will be called as 'the SOC region'. Moreover, we can see that the Hurst parameter quickly decays from the radial position $r/a = 0.95$ towards inside the plasma column (plasma edge). The same situation is observed for Hurst parameter that decreases in the scrape-off layer plasma according to the radial position moving away from $r/a = 1.1$ to out of the plasma column. The variation of the TCABR Hurst values is from 0.57 (on border of the figure) to maximum value 0.83 around the limiter ($r/a = 1$). Such scenario indicates that the plasma turbulence and probably the plasma transport present high self-organized similarity behavior [13]. The SOC behavior more pronounced close to radial positions just after the limiter is an indication of high spatial correlations in this region. Complementary, the observed SOC decrease towards internal or external regions indicates a turbulence decorrelation that may be caused by the high shear flow present in these regions.

The features reported in this section are an indication of SOC at the plasma edge. However, alternatively, some of these features could also be explained by other dynamical models. Thus, for example, high Hurst parameter values could also be interpreted as an indication of coherent structures caused by coherent drift waves traveling poloidally at the plasma edge.

4. Self-organized criticality during MHD driven turbulence

In the TCABR, when the MHD activity increases the high MHD activity synchronizes with the electrostatic fluctuations and their frequency spectra have the same peaks [25,22]. The high MHD activity modifies the plasma turbulence leading to a new dynamic scenario on the plasma edge [33]. In this section we determine the influence of the high MHD activity on SOC dynamics.

Thus, we analyze the SOC behavior of the electrostatic fluctuations on time interval with high MHD activity. To perform it, we analyzed the fluctuation signal filtering the dominant MHD frequency. The filter is as follows: first we apply the Fourier transform

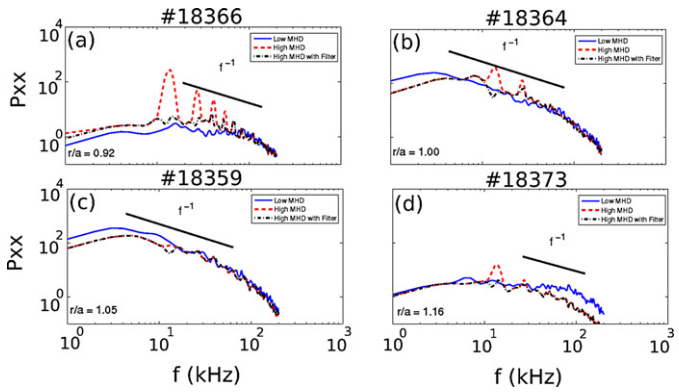

Fig. 5. Power spectrum of the floating potential fluctuation at four different radial positions: (a) $r/a = 0.92$ (inside the plasma column); (b) $r/a = 1$ (limiter); (c) $r/a = 1.05$ and (d) $r/a = 1.16$ (outside the plasma column), respectively. For all four figures we have the power spectrum with low MHD activity (blue continuous line), with high MHD activity (red dashed line) and with MHD high activity filtered the resonants frequencies (black dashed line). (For interpretation of the references to color in this figure, the reader is referred to the web version of this Letter.)

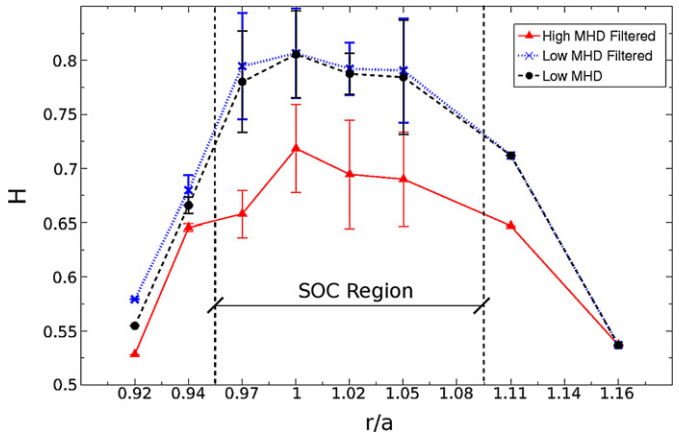

Fig. 6. (Color online.) Radial dependence of the Hurst parameter in time range with low MHD activity (circles), high MHD activity filtered (triangles) and low MHD activity filtered (asterisks) with the same spectral range used in high MHD activity. The vertical black dashed lines marks the position of the existence of SOC behavior radial dependence.

and observe the MHD modes in the power spectrum, as shown in Fig. 5 with high MHD activity (red dashed line). Then, we extract the signal with the dominant frequency 13 kHz and their harmonics. The influence of the oscillations induced by the MHD modes on the floating potential signals is removed by using a numerical spectral filter. To do it, initially we perform a Fourier transform of the original signal. Then, we decrease the amplitude of the Fourier coefficients in the frequencies in the range of the main MHD peak and their harmonics to almost zero and finally we perform the inverse Fourier transform. This procedure corresponds to have a band-stop filter (or band-reject filter). To verify the SOC dynamics of the extracted signal, we obtain its power spectrum and Hurst parameter.

In Fig. 5 we present the power spectra of the floating potential fluctuation at four radial positions, $r/a = 0.92$, 1.0, 1.05, and 1.16. Each one of the four plots in Fig. 5 show the power spectra with low MHD activity (blue continuous line), with high MHD activity (red dashed line), and with MHD high activity filtered at the resonant frequencies (black dashed line).

Fig. 6 exhibits the radial profiles of the Hurst parameters estimated from potential fluctuations at various radial positions including the SOC region: low MHD activity (circles), low MHD activity filtered (asterisks) and high MHD activity filtered (triangles). It

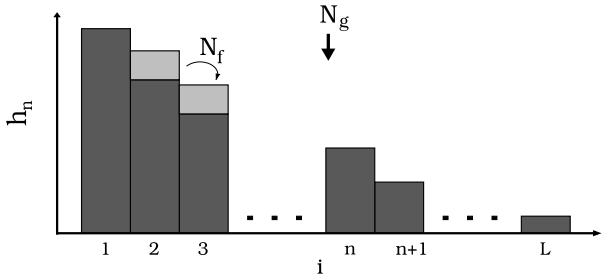

Fig. 7. The one-dimensional sandpile model with L cells versus height h_n, where n is each lattice site, N_f is the number of sand grains that slide off the sandpile slope and N_g is the number of sand grains randomly deposited at each time.

is noted that at the radial positions around the plasma limiter the Hurst parameters are well above 0.5, indicating the existence of long-range dependencies in the fluctuation dynamics in the plasma edge SOC region. Moreover this figure shows a decreasing of Hurst parameters in the SOC region when the MHD activity increases.

The fact that the filtered signal (with high MHD activity) and the signal with low MHD activity have different SOC indicators shows that the high MHD activity changes the dynamics of turbulence in the plasma edge region [12]. We interpreted this fact by the nonlinear coupling between high MHD activity and plasma turbulence. We conjectured that a nonlinear coupling modifies the turbulence breaking out the SOC dynamics. In fact, if we assumed that there is no coupling between the turbulence and the MHD activity, the effects of the high MHD activity would be restricted to the frequency of the MHD modes and the filtered signal would have the same characteristics of the signals without high MHD, which is not observed. The present results show that the high MHD activity in TCABR reduces, but not suppresses, the self-organized criticality at the plasma edge.

5. Sandpile model

In this section we consider a sandpile model to simulate the reported SOC experimental evidence on turbulence data analyzed in this work. A cellular automaton is used to study the sandpile behavior. We have modified the one-dimensional model implemented by Hwa and Kardar [34]. The domain is separated into cells, where N_g sand grains are added to the cells with a determined probability. So, we apply the following rule: if $Z_n \geqslant Z_c$, then $h_n = h_n - N_f$, and $h_{n+1} = h_{n+1} + N_f$, where h_n is the height of the cell n, Z_n is the difference between h_n and h_{n+1}, Z_c is the critical gradient and N_f is the amount of sand that falls in an overturning event (Fig. 7).

A method to quantify self-organized criticality is the frequency diagnostics applied to the time history of instantaneous flips considering the saturated region. The frequency spectrum can be divided into three regions. The first region is the high-frequency end of the spectrum, that follows approximately a f^{-4} power law (right region). This region is identified as the no interacting (overlapping) avalanche region. The intermediate region presents a f^{-1} dependence that is related to transport events linked with SOC characteristics. In the third region the spectral power is relatively flat and finally rolls over at the lowest frequencies. This last region is identified with global discharge events that have extremely long correlation times.

Fig. 8(a) shows the power spectrum for data obtained of the TCABR and Fig. 8(b) for sandpile model with $L = 200$. The black line corresponds to the condition where the MHD activity is low, while the red line is for high MHD. It is possible to simulate the high MHD (red line) due to the fact that we added an external particle driving N_{ext} in the sandpile model. The external driving is an amount of sand that falls in a determined time τ. The grains

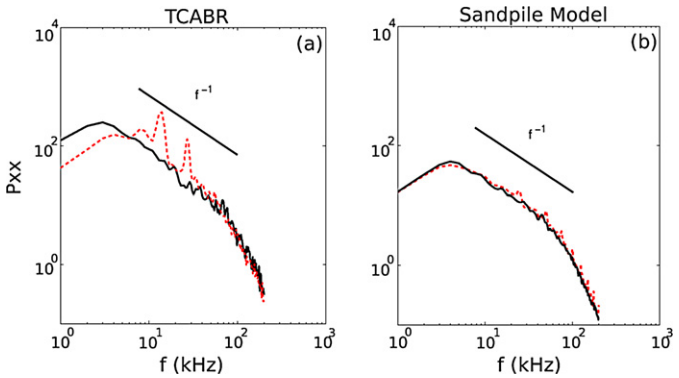

Fig. 8. Power spectrum of the floating potential fluctuation (a) and sandpile model (b) with (red) and without (black) high MHD activity. In the sandpile model we consider $L = 200$, $N_f = 3$, $N_g = 3$, $Z_c = 8$, $\tau = 47$, 1.1 10^6 iterations and 1.0×10^6 transient iterations. In our simulations we consider $N_{ext} = 0$ to obtain black line and $N_{ext} = 40$ to red line. (For interpretation of the references to color in this figure, the reader is referred to the web version of this Letter.)

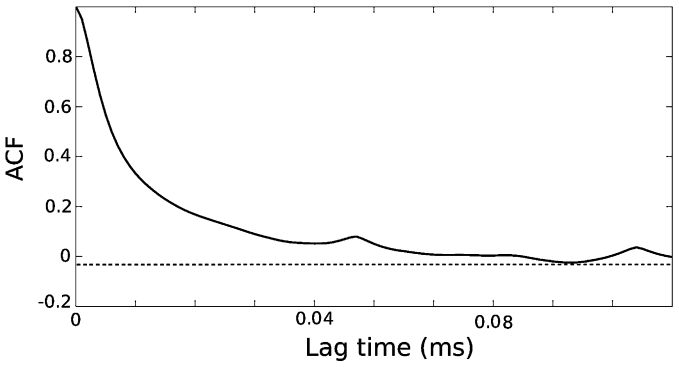

Fig. 9. Autocorrelation function (ACF) of the sandpile model for $L = 200$, $N_f = 3$, $N_g = 3$, $Z_c = 8$, $N_{ext} = 40$, $\tau = 47$, 1.1×10^6 iterations and 1.0×10^6 transient iterations.

are added at random sites. Besides, there is the sand N_g that fall in an overturning. It is possible to obtain other value of the peak frequency in Fig. 8(b) varying N_{ext} and τ.

The autocorrelation function for the sandpile model with external driving from numerical simulation is displayed by Fig. 9. Our modified model reproduces the same behavior observed in Fig. 3(b) and (c), that is, the existence of long time correlations. Moreover, we obtain the Hurst parameter equal to 0.7.

6. Conclusion

In conclusion, our analyzes of floating potential fluctuation data from TCABR tokamak point out evidences of SOC behavior at the TCABR plasma edge. Moreover, we also find that this SOC behavior is more pronounced close to radial positions just after the limiter. We also find that during the high MHD activity the Hurst parameter of the electrostatic turbulence decreases in all frequency range, which suggests a coupling between the resonant magnetic oscillations and the broad band electrostatic fluctuations.

Moreover, in this work we also use a cellular automaton (sandpile model) to reproduce the main SOC characteristics observed in the analyzed data. In a first step we choose the parameters of the sandpile model to describe the frequency spectra of the TCABR turbulence in a condition with low MHD activity. In a second step, we introduced a periodical external driving in the sandpile model to reproduce the spectral features observed during discharges with high MHD activity.

Thus, this work confirmed previous evidences of SOC dynamics in tokamak plasma edge turbulence and determined its radial dependence. Furthermore, the effect of high MHD activity on the electrostatic turbulence SOC dynamics was also studied. Finally, we verified that the SOC dynamics observed in the experimental data with high MHD activity are compatible with the dynamics of a cellular automaton composed by a sandpile model with periodical external driving.

Acknowledgements

This work was made possible through partial financial support from the following Brazilian research agencies: CNPq, CAPES, FAPESP and Fundação Araucária.

References

[1] J. Wesson, Tokamaks, 3rd ed., Oxford University Press, 2004.
[2] A.H. Boozer, Rev. Modern Phys. 76 (2005) 1071.
[3] W. Horton, Rev. Modern Phys. 71 (1999) 735.
[4] P.J. Morrison, B.A. Shadwick, CNSNS 13 (2008) 130.
[5] M.S. Baptista, I.L. Caldas, M.V.A.P. Heller, A.A. Ferreira, R. Bengtson, J. Stöckel, Physics of Plasmas 8 (2001) 4455.
[6] E.G. Altmann, E.C. Silva, I.L. Caldas, Chaos 14 (2004) 975.
[7] Z.O. Guimarães-Filho, I.L. Caldas, R.L. Viana, I.C. Nascimento, Yu.K. Kuznetsov, J. Kurths, Physics of Plasmas 17 (2010) 012303.
[8] Y.H. Xu, S. Jachmich, R.R. Weynants, A. Huber, B. Unterberg, U. Samm, Physics of Plasmas 11 (2004) 5413.
[9] C.R. Neto, Z.O. Guimarães-Filho, I.L. Caldas, I.C. Nascimento, Yu.K. Kuznetsov, Physics of Plasmas 15 (2008) 082311.
[10] F. Sattin, M. Baiesi, Phys. Rev. Lett. 96 (2006) 105005.
[11] P. Bak, C. Tang, K. Wiesenfeld, Phys. Rev. Lett. 59 (1987) 381384.
[12] P. Bak, C. Tang, K. Wiesenfeld, Phys. Rev. A 38 (1988) 364374.
[13] D.E. Newman, B.A. Carreras, P.H. Diamond, T.S. Hahm, Physics of Plasmas 3 (1996) 1858.
[14] E.A. Reis, L.B.L. Santos, S.T.R. Pinho, Physica A 388 (7) (2009) 1303.
[15] S. Das, Chaos Solitons Fractals 44 (4–5) (2011) 185.
[16] L.S. Furtado, M. Copelli, Phys. Rev. E 73 (2006) 011907.
[17] A. Manor, N.M. Shnerb, Phys. Rev. Lett. 101 (2008) 268104.
[18] J.E. Keymer, P.A. Marquet, A.R. Johnson, J. Theoret. Biology 194 (1) (1998) 79.
[19] H. Punzmann, M.G. Shats, Complexity International 12 (2005) 1.
[20] I.C. Nascimento, Yu.K. Kuznetsov, Z.O. Guimarães-Filho, I. El Chamaa-Neto, O. Usuriaga, A.M.M. Fonseca, R.M.O. Galvão, I.L. Caldas, J.H.F. Severo, I.B. Semenov, C. Ribeiro, M.V.P. Heller, V. Bellintani, J.I. Elizondo, E. Sanada, Nucl. Fusion 47 (2007) 1570.
[21] Z.O. Guimarães-Filho, I.L. Caldas, R.L. Viana, M.V.A.P. Heller, I.C. Nascimento, Yu.K. Kuznetsov, R.D. Bengtson, Physics of Plasmas 15 (2008) 062501.
[22] G.Z. dos Santos Lima, Z.O. Guimarães-Filho, A.M. Batista, I.L. Caldas, S.R. Lopes, R.L. Viana, I.C. Nascimento, Yu.K. Kuznetsov, Physics of Plasmas 16 (2009) 042508.
[23] R.M.O. Galvão, Yu.K. Kuznetsov, I.C. Nascimento, E. Sanada, D.O. Campos, A.G. Elfimov, J.I. Elizondo, A.N. Fagundes, A.A. Ferreira, A.M.M. Fonseca, E.A. Lerche, R. Lopez, L.F. Ruchko, W.P. de Sá, E.A. Saettone, J.H.F. Severo, R.P. da Silva, V.S. Tsypin, R. Valencia, A. Vannucci, Plasma Physics and Controlled Fusion 43 (9) (2001) 1181.
[24] I.C. Nascimento, Yu.K. Kuznetsov, J.H.F. Severo, A.M.M. Fonseca, A. Elfimov, V. Bellintani, M. Machida, M.V.A.P. Heller, R.M.O. Galvão, E.K. Sanada, J.I. Elizondo, Nucl. Fusion 45 (2005) 796.
[25] Z.O. Guimarães-Filho, G.Z. dos Santos Lima, I.L. Caldas, R.L. Viana, I.C. Nascimento, Yu.K. Kuznetsov, J. Phys.: Conference Series 246 (2010) 012014.
[26] V. Carbone, G. Regnoli, Physics of Plasmas 7 (2000) 445.
[27] P.A. Politzer, Phys. Rev. Lett. 84 (2000) 1192.
[28] E. Spada, V. Carbone, R. Cavazzana, L. Fattorini, G. Regnoli, N. Vianello, V. Antoni, E. Martines, G. Serianni, M. Spolaore, L. Tramontin, Phys. Rev. Lett. 86 (2001) 3032.
[29] G.Z. dos Santos Lima, K.C. Iarosz, A.M. Batista, Z.O. Guimarães-Filho, I.L. Caldas, Yu.K. Kuznetsov, I.C. Nascimento, R.L. Viana, S.R. Lopes, J. Phys.: Conference Series 285 (2011) 012004.
[30] B.A. Carreras, B. van Milligen, M.A. Pedrosa, R. Balbin, C. Hidalgo, D.E. Newman, E. Sanchez, M. Frances, I. Garcia-Cortés, J. Bleuel, M. Endler, S. Davies, G.F. Mathews, Phys. Rev. Lett. 80 (1998) 4438.
[31] R. Sánchez, D.E. Newman, B.A. Carreras, Nucl. Fusion 41 (2001) 247.
[32] R. Sánchez, D.E. Newman, B.A. Carreras, Phys. Rev. Lett. 88 (2002) 068302.
[33] R.L. Viana, S.R. Lopes, I.L. Caldas, J.D. Szezech Jr., Z.O. Guimarães-Filho, G.Z. dos Santos Lima, P.P. Galuzio, A.M. Batista, Yu.K. Kuznetsov, I.C. Nascimento, Communications in Nonlinear Science and Numerical Simulation (2011), doi:10.1016/j.cnsns.2011.07.006.
[34] T. Hwa, M. Kardar, Phys. Rev. A 45 (10) (1992) 7002.